EPJ AP

Applied Physics

EPJ.org

your physics journal

Eur. Phys. J. Appl. Phys. (2014) 67: 30801 DOI: 10.1051/epjap/2014140137

Experimental and numerical investigations of the corona characteristics of a new Tri-electrode system for electrostatic separation processes

Mohamed M. Abouelsaad, Mohamed A. Abouelatta, and Abdelhadi R. Salama

edp sciences

The title “The European Physical Journal” is a joint property of EDP Sciences, Società Italiana di Fisica (SIF) and Springer

Eur. Phys. J. Appl. Phys. (2014) 67: 30801
DOI: 10.1051/epjap/2014140137

THE EUROPEAN PHYSICAL JOURNAL
APPLIED PHYSICS

Regular Article

Experimental and numerical investigations of the corona characteristics of a new Tri-electrode system for electrostatic separation processes

Mohamed M. Abouelsaad[a], Mohamed A. Abouelatta, and Abdelhadi R. Salama

Faculty of Engineering at Shoubra, Benha University, 108 Shoubra st., Cairo, Egypt

Received: 4 April 2014 / Received in final form: 12 June 2014 / Accepted: 17 June 2014
Published online: 13 August 2014 –

Abstract. The paper presents the measurement and computation of the corona onset voltages, electric field and ion current density profiles of a new "Tri-electrode system" intended for electrostatic separation applications. Unlike the well-known "dual cylinder-wire electrode system", the new system utilizes an extra adjustable wire in order to provide the means for a more efficient ion charging current; necessary for separation of different granular mixtures. An experimental setup is constructed to model the present multi-electrode arrangement. The measurements are carried out for wire diameters between 0.3–1.0 μm and for different geometrical parameters. Without resorting to the commonly used Deutch's assumption, a computational scheme is developed to solve the corona equations and to compute the associated ionized field quantities of the system. Mapping of the ion flow field patterns demonstrates the impact of this assumption on the solution's accuracy. The computed results were found to be in good agreement with experiments. The configuration offers a more efficient charging process and separation in comparison with earlier separators' designs.

1 Introduction

Electrostatic separation of granular mixtures of materials, spraying of powders or neutralization of charged insulating materials are just a few of the electrostatic applications processes relying on the corona discharge phenomena [1–3]. Several ionizing electrodes' shapes and types for electrostatic separation processes; including needles, wires or blades, have been proposed and presented in literature [4–6]. The efficiency of corona charging processes, utilized in electrostatic separation, usually depends on a multitude of factors including the level and polarity of the high-voltage supply as well as on the different geometrical parameters of the electrode system. Significant efforts and research have been carried out to characterize the various types of electrodes and to compute their corona onset voltage V_o, electric field strength E, as well as the generated ionic current density J [7–15].

A widely-used electrode type for electrostatic separators is the dual wire-cylinder corona electrode where a high-intensity electric field is generated between a grounded roll electrode and a high voltage dual electrode consisting of an ionizing wire attached to a non-ionizing cylindrical. The particles to be sorted are fed onto the surface of the grounded electrode to be exposed to the high electric field zone. The ionizing wire creates a corona discharge and all the particles are charged by ion bombardment. The charged insulating particles adhere to the surface of the grounded electrode by the electric image force to be later removed to fall freely in a collecting system. The conducting particles, upon contact with the grounded electrode, lose their charges. Under the action of the electric field, they get charged by electrostatic induction and are projected towards the static electrode of opposite polarity [7–15].

The geometrical parameters of the dual wire-cylinder electrode as well as the applied voltage are known to largely influence the separator's operation [16,17]. The cylindrical non-ionizing metallic electrode; besides its role as a mechanical support, has a significant influence on the onset and development of the corona discharge. However, due to the very limited space of the separator, little control is usually possible over these geometrical parameters and consequently over the corona onset voltage, ground-level current density and other important characteristics of the separator. The modification of corona electrode by connecting a metallic cylinder in parallel with the energized wire was suggested as a solution to modulate the charging process of non-woven filter media [17,18]. In another study, the impact of electrode asymmetry on the effectiveness of corona discharge applied in order to neutralize the charge deposited on the

[a] e-mail: mabouelsaad@yahoo.com

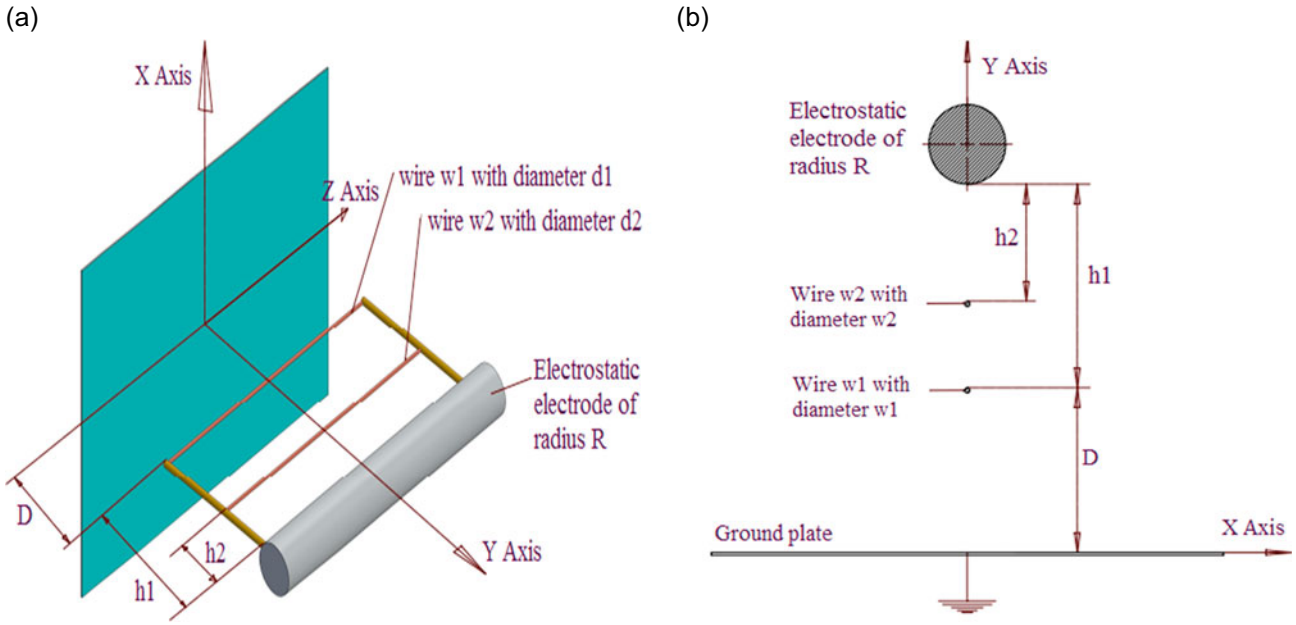

Fig. 1. (a) Tri-electrode configuration, (b) 2-d representation of the electrode system in (a).

surface of granular insulating materials was evaluated and assessed [19]. Recently, a new Tri-electrode system has been introduced, shown in Figure 1 [20]. Such a design would allow a wide and smooth control of the corona onset voltage through the insertion of an adjustable auxiliary wire W_2 in the gap between the ionizing wire W_1 and the cylinder; being parallel to them and having the same voltage. The proposed design takes advantage of the electric field modulation at the surface of the ionizing wire in order to provide flexible control over the corona performance of the separator.

The paper aims to quantify the corona performance of the proposed Tri-electrode configuration including the onset voltage as well as the electric field and current density distributions at the surface of the grounded electrode. The role of the adjustable auxiliary wire in modulating the surface field of the ionizing wire and switching on/off of the discharge is examined both experimentally and numerically. The results are analyzed and discussed to assess the influence of the geometrical characteristics of the proposed electrode configuration and to evaluate the system's merits which would lead to the most efficient charging process and separation.

2 Corona model of the Tri-electrode system

2.1 Physical model

The corona discharge, for any shape or type of ionizing electrode, is usually characterized by the presence of two regions: an ionizing thin layer, very close to the active electrode surface, and a drift zone where the ions are driven by the field toward a collecting electrode. To simplify modeling the corona discharge, the ionizing thin layer is considered as the only source of unipolar ions and the study of corona discharge is reduced to the evaluation of the space charge density due to the unipolar ions which move along the field lines. This approach is generally suitable to model the corona electric field, as affected by the ionic space charge [21].

The ionizing wire W_1, the movable auxiliary wire W_2 and the electrostatic cylinder are all at the same applied negative potential V. The plate is connected to the ground. The corona discharge is assumed to take place only at the surface of the wire W_1 (i.e., ionizing electrode). Both the auxiliary wire W_2 and the cylindrical electrode are assumed to be in non-ionizing state. The physical model of the corona discharge adopted for the present study assumes that the unipolar ions leave the surface of the ionizing wire W_1 and move toward the grounded plate in the combined field established by the three electrodes with constant mobility k. The electrodes are placed in air such that $D = \varepsilon_0 E$, D and E being the electric displacement and field strength, respectively, and ε_0 the vacuum permittivity.

2.2 Governing equations and boundary conditions

The computation domain is assumed to be two-dimensional; neglecting the edge effects of the electrodes and considering that the corona discharge is constant and uniform all along each cylindrical wire thus the coupled electric field and space charge distributions would be 2-dimensional. The governing equations describing the electric field E in the presence of the negative ions are as follows:

Poisson equation:

$$\Delta V = -\rho/\varepsilon_0, \tag{1}$$

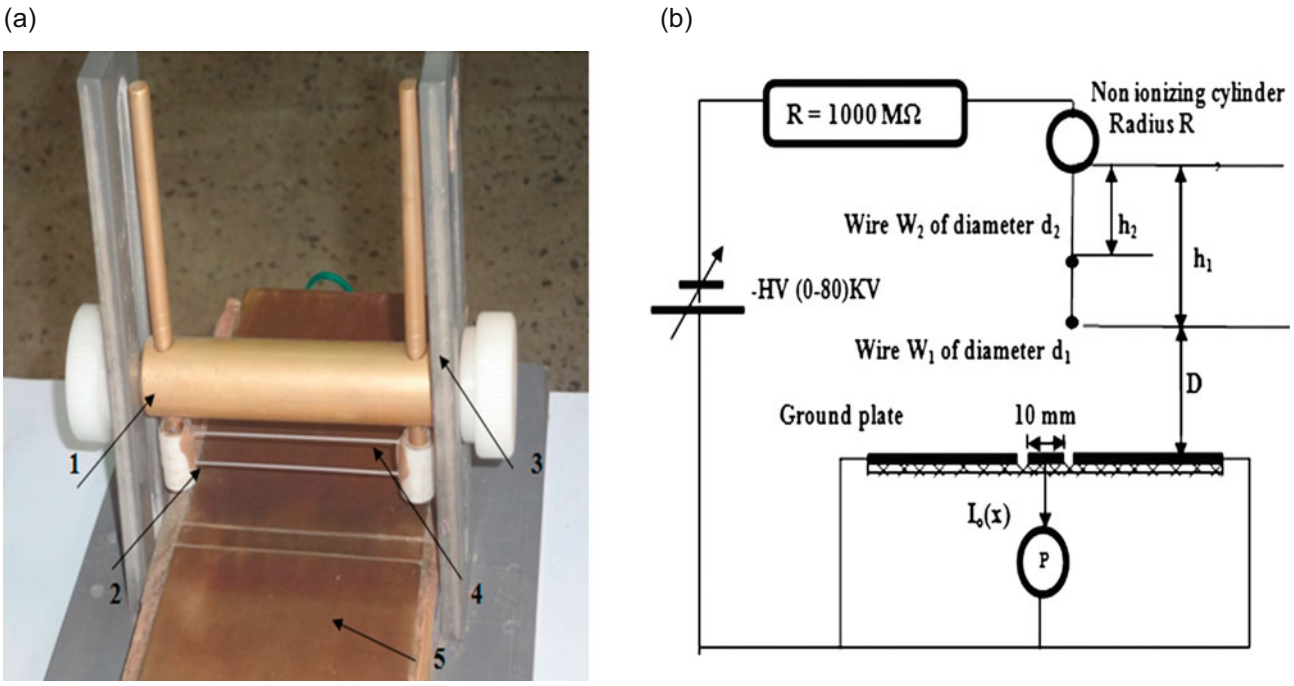

Fig. 2. Experimental setup of the geometry of the Tri-electrode system. (1) Non ionizing cylinder, (2) ionizing wire W_1, (3) insulating support, (4) adjustable auxiliary wire W_2, (5) ground plate.

where ρ is the ionic space charge density and V is the electric potential and,

electric field:

$$E = -\nabla V. \tag{2}$$

The current continuity equation:

$$\nabla \cdot j = 0, \tag{3}$$

where $j = \rho k E$ is the corona current density and k is the ion mobility in m^2/Vs. For the electrical potential (Poisson equation), the boundary conditions are of Dirichlet type for all electrodes (the wire W_1, the auxiliary wire W_2 and the non-ionizing electrode) with potential V and the collector plate will be grounded. The space charge-free electric field is represented by Laplace's equation:

$$\Delta V = 0. \tag{4}$$

For the continuity equation (3), the boundary condition consists in imposing a charge density value at all emitting points on the wire surface $\rho_0(\Omega)$. The method that permits to establish the value of $\rho_0(\Omega)$ at each emitting point is based on the Kaptzov's assumption and Peek's relation [22]:

$$E_P = 31\,\delta(1 + 0.308/r^{1/2}), \tag{5}$$

where E_P is the corona onset field in kV/cm, δ is the air density and r is the radius of the wire in cm. Therefore, the boundary condition for the current continuity equation (3) is replaced by the Kaptzov's condition that the electric field E at any point Ω on the surface of the ionizing electrode remains constant and equals the Peek's field when voltage is increased beyond the corona onset level, i.e., $E(\Omega) = E_P$.

The electric field strength of the ionizing wire is influenced not only by the presence of the cylindrical electrode, but also by the presence of the auxiliary wire W_2. The boundary condition of the continuity equation i.e., $\rho_0(\Omega)$ must be adjusted in order to reflect this field modulation. The condition that the electric field $E(\Omega)$ equals E_P will be assigned, for any point Ω on the wire surface, in order to simulate the dependence of the value of the charge density on of the position of the point Ω. Any point on the ionizing wire will be considered to emit charges only if the local field strength takes a value higher than that given by Peek's relation E_P.

3 Experimental procedure and measurements

The experimental set-up for the measurement of onset voltage, current-voltage characteristics of the corona wire and for the study of the corona current density distribution at the surface of the grounded plane electrode is shown in Figures 2a and 2b. The basic configuration consists of two tungsten wires of the same diameter (between 0.3 and 1.0 mm each), both strung parallel to and above a rectangular copper plane-electrode of dimensions 300 mm × 100 mm. The distances are $h_1 = 20$ mm, $h_2 = 10$ mm and $D = 25$ mm respectively. For current density measurements, a current probe (a copper strip 100 mm × 10 mm), electrically insulated from the rest of the grounded electrode and connected to a microammeter, is used. The electrodes were energized from a negative DC a high-voltage supply (Hipotronics model

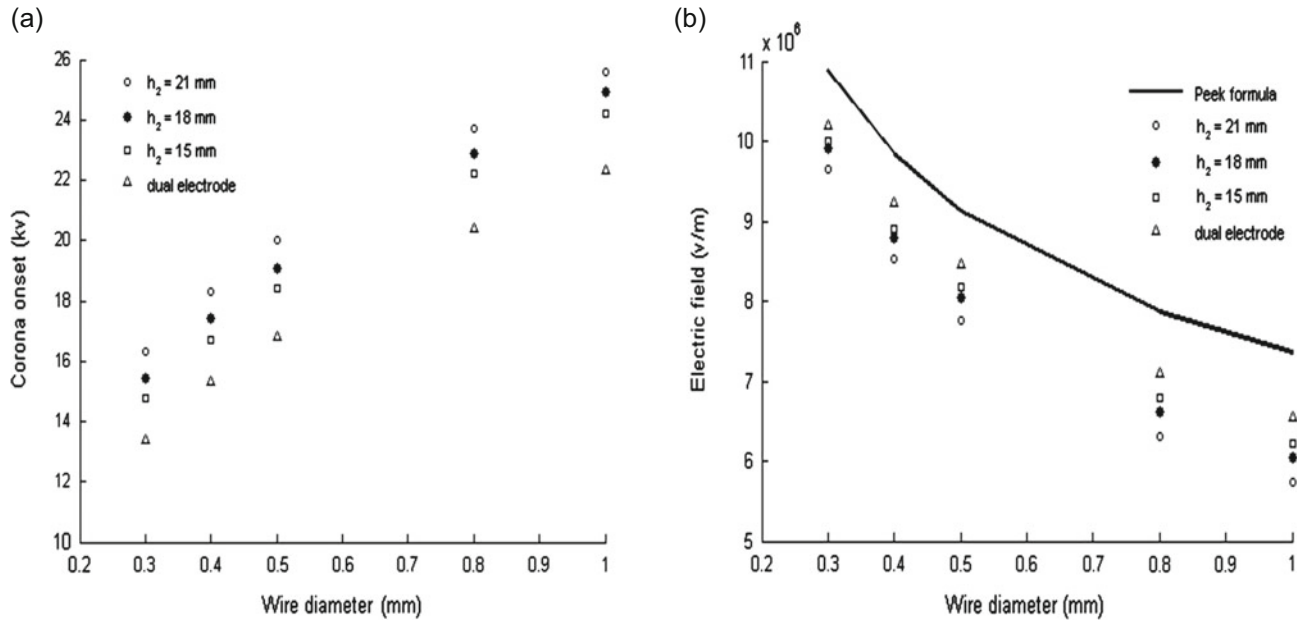

Fig. 3. Corona onset characteristics for different wire diameters, $h_1 = 25$ mm. (a) Experimental corona onset voltage, (b) computed electric field strength at onset.

800pl-10mA, 0–80kV). The corona onset voltage is determined as the voltage for which the reading of the microammeter P (connected between the collecting plate and the ground, Fig. 2b) increases by one order of magnitude.

The measured corona onset voltages are presented in Figures 3a and 4a for different wire diameters. For each arrangement, the electric field strength at the wire surface upon corona onset is determined and compared with those computed using Peek's formula in Figure 3b and 4b. If V_0 is the corona onset voltage determined experimentally for the given geometry, then the corresponding electric field on the corona wire at onset can be calculated as $E_0 = E_P(V_0/V)$ where V, calculated using the GA/CSM algorithm, is the voltage which produces an electric field strength of a magnitude E_P at the surface of the wire W_1 [9,11].

Inspection of these results show that the corona onset voltage decreases with the decrease of the wire diameter. As the auxiliary wire moves upward (h_2 decreases), the corona onset voltage decreases and vice versa. Variations in the corona onset voltage were observed to be larger for smaller wire diameters and also for smaller h_1 (i.e., the non-ionizing cylinder is close to the ionizing wire). For the case $h_1 = 25$ mm, a variation in the corona onset level of about 10% is observed for $d_1 = 0.3$ mm and about 6% for $d_1 = 1.0$ mm as h_2 varies between 60% and 80%. Similarly, for the case $h_1 = 15$ mm, a variation of about 11.4% is observed for $d_1 = 0.3$ mm and about 7% for $d_1 = 1.0$ mm as h_2 varies between 30% and 70%, Figures 3a and 4a. It is also observed that the electric field strength at corona onset, Figures 3b and 4b are lower than the values predicted by Peek's formula. These results are in agreement with the findings of [9,11] where it was reported that a correction factor should be applied to Peek's formula for such small wire diameters and multi electrode arrangement. The presence of the auxiliary wire significantly modifies the distribution of the electric field close to the ionizing wire of the present Tri-electrode system. Another observation is that when the cylindrical electrode was positioned closer to the ionizing wire, $h_1 = 15$ mm, Figure 4, the corona onset voltage increases and the corresponding electric field decreases as compared to the case of $h_1 = 25$ mm shown in Figure 3. These variations of the onset level are 11% for $d_1 = 0.3$ mm and about 6% for $d_1 = 1$ mm respectively. In other words, the presence of the auxiliary wire, in this case, may be more effective for smaller wire diameters and closeness of the cylindrical electrode to the ionizing wire. It should be noted that the onset voltages observed were between 9% and 20% higher than that of the corresponding dual electrode system levels which should be reflected in the selection of the rating of the high voltage supply. The distance between the two wires $(h_1 - h_2)$ was kept constant when comparing the different cases.

4 Space charge-free electric field (GA-CSM algorithm)

The calculation of the space-charge-free electric field, equation (4), of the proposed electrode arrangement, Figure 1, is the first step in the solution of the ionized field problem. The charge simulation method (CSM) is employed to calculate the symmetrical 2-D field with the above boundary conditions [10]. A set of N_g simulating line charges is placed adjacent to the energized electrodes' inner surfaces with a similar number of boundary points selected along these surfaces. According to the CSM, a matrix equation (6) is set up and solved to determine the

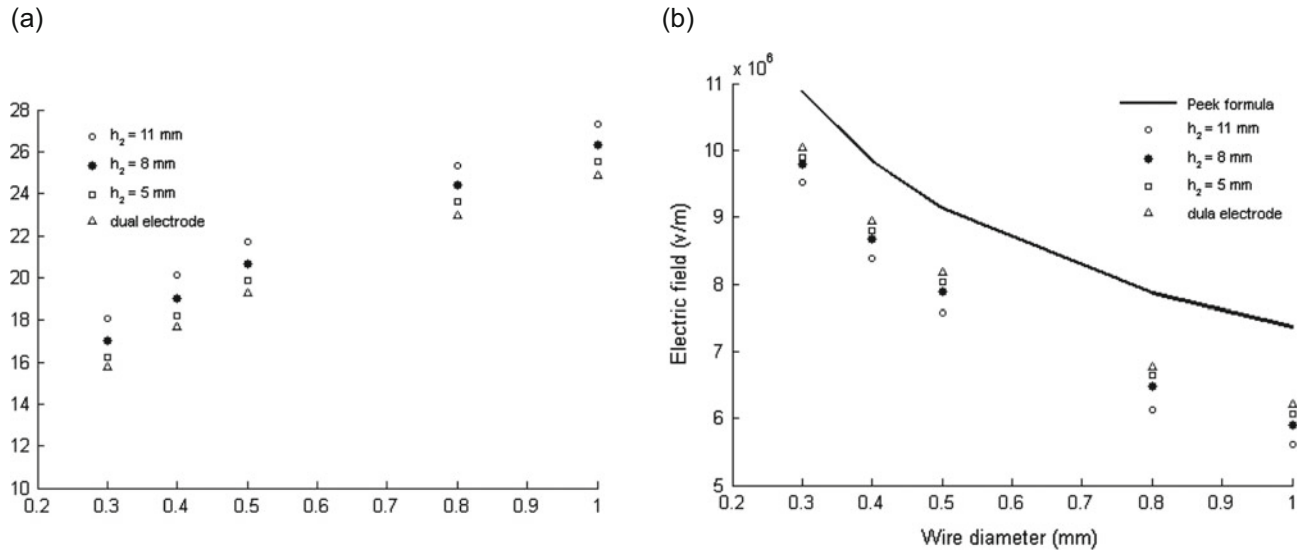

Fig. 4. Corona onset characteristics for different wire diameters, $h_1 = 15$ mm. (a) Experimental corona onset voltage, (b) computed electric field strength at onset.

magnitude of the simulation charges Q:

$$[P][Q] = [V], \tag{6}$$

$$[F_X][Q] = [E_X], \tag{7}$$

$$[F_Y][Q] = [E_Y], \tag{8}$$

where P is the potential coefficient matrix, Q is the column vector of unknown charges; V is the column vector of known potentials at the contour points. F_X and F_Y are the electric field intensity coefficients between the simulation charges and the electric field intensity components at the point where this field is required; in a Cartesian coordinate system. E_X and E_Y are the components of the electric field intensity at the same point. The coefficients P will be determined by the location of the charges and the contour points.

A set of 20 simulating line charges are placed inside the ionizing wire W_1, wire W_2 and the cylindrical electrode on hypothetical cylindrical surfaces of diameters $d_1 \times C_1$, $d_2 \times C_2$ and $2R \times C_3$ respectively; with the charges being parallel to each electrode surface. Three optimization parameters C_1, C_2, C_3, with values ranging between 0 and 1.0, are considered. The image method is used to simulate the ground plate. An algorithm which couples genetic algorithms and the charge simulation method (GA/CSM program) is developed in the MATLAB environment in order to determine the optimal values of the parameters C_1, C_2 and C_3 such that the accumulated square error (ASE) of the potential values along all the electrodes' surfaces is minimized [10]:

$$FF = \sum_{j=1}^{N_h} [V - v_j]^2, \tag{9}$$

where V is the electrode voltage of the ionizing wire, the auxiliary wire and the non-ionizing cylinder, and $V_j = \sum_{i=1}^{n} P_{ji} Q_i (j = 1, 2, \ldots N_h)$ is the potential obtained by the CSM at the check point j, and N_h is the total number of check points. Implementation of the GA-CSM algorithm is as follows [10]:

1. Determine the domain for the optimization parameters.
2. GA generates initial uniform random values for C_1, C_2, C_3.
3. For each call to the CSM routine by GA, the CSM will produce the ASE error for this set of optimization parameters.
4. The GA will then evaluate the fitness function and modify the optimization parameters to minimize the ASE error.
5. Steps 3–4 are repeated for a pre-specified number of generations.

4.1 Field modulation around the ionizing wire

For the wire-cylinder dual electrode, earlier studies of the electric field and ion current density showed that the geometrical characteristics of the arrangement play a very important role for the separator's operation in order to ensure an efficient particle charging process and a maximum field strength along the grounded electrode [7–9]. In fact, as the large non-ionizing cylinder gets closer to the wire, the corona onset voltage of the wire increases, resulting in lower charge emission and vice versa [7–9]. So, it is possible to obtain higher or lower current without changing the gap D and the applied voltage through the adjustment of the wire-cylinder clearance, for each mixture, to obtain suitable ionic current distribution and maximum particle charging. However, the use of relatively large wire-cylinder clearance, of the dual electrode system, is rather limited in view of the overall small size of the separator. The Tri-electrode configuration overcomes these limitations and provides a more flexible control of the separator's operation as will be demonstrated in the following sections.

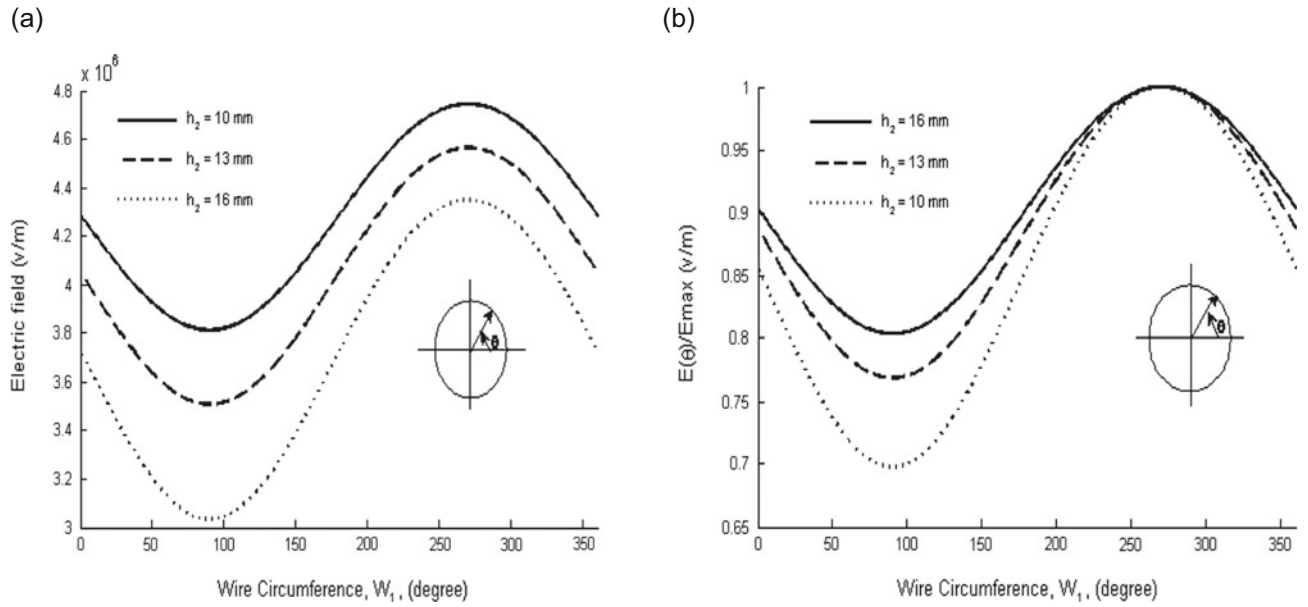

Fig. 5. Electric field modulation around the wire W_1 for different locations of the auxiliary wire h_2 ($V = 10$ kV, $d_1 = d_2 = 0.5$ mm, $D = 25$ mm, $h_1 = 20$ mm). (a) Variation of electric field, (b) per unit variation of electric field.

The GA-CSP program is utilized to compute the electric field strengths E_1 at surface of the wire W_1. The effectiveness of the presence of the auxiliary wire on modulating the electric field around the ionizing wire surface is demonstrated in Figure 5a. It is clear that as the auxiliary wire W_2 gets closer to the wire W_1, the surface field on W_1 decreases and becomes more nonuniform. The field at the top of the wire surface is more affected than that at the bottom as shown in Figure 5b, and the corona onset voltage will vary accordingly. This means that by properly positioning the auxiliary electrode, both the corona onset voltage and the level of ionization can be smoothly varied and controlled. In fact, the wire W_1 can be switched to be in an ionizing or non-ionizing state, with all other parameters being the same, by simply positioning the wire W_2 either closer or farther away from W_1. The proposed electrode configuration may thus be termed "switchable dual electrode".

5 Computational scheme of the ion flow fields (MOC/CSM algorithm)

Several methods had been earlier developed to solve the corona governing equations for different geometries [12,13,23–27]. The present study extends the application of the coupled technique of the method of characteristics and the charge simulation method (MOC/CSM) to solve the corona problem of the proposed Tri-electrode configuration described by equations (1)–(3). The charge simulation method is used to solve equations (1) and (2), while the method of characteristics (MOC) is employed to solve equation (3). Both problems are solved iteratively until the solution of the system of equations is reached (the values of V, E, ρ and $\rho_0(\Omega)$ are obtained for all the points of the domain). The method aims to achieve a self-consistent solution of the problem i.e., simultaneously establishing a self consistent electric field and a self consistent space charge distribution. A two-loop algorithm is developed is developed for this purpose. Within the inner loop, the spatial distributions of the electric field and space charge density are updated at the end of the loop. The computational process continues with the charge distribution, at any point on the wire surface, being modified in an outer loop until the computed field on the wire surface equals the onset value. The boundary conditions of the problem are the following:

1. All points along the non ionizing cylinder, wire W_1 and wire W_2 surfaces have a potential equal to the applied voltage.
2. All points along the surface of the plate are at zero potential.
3. The electric field of is equal to the onset field at all points on the surface of the corona ionizing wire W_1.

The algorithm steps are as follows [28]:

1. Input the data: geometrical dimensions, applied voltage, corona onset field.
2. Compute the wire surface charges, space charge-free case, using the GA-CSM.

Following these steps, two loops are then developed as follows:

3. Generate a grid of elements made by the intersection of the characteristic lines and equipotential contours.
4. Compute the charge density at the grid points by the method of characteristics. Determine the corresponding space charges within each element.
5. Modify the surface charges to satisfy the Dirichlet boundary conditions at all electrodes.

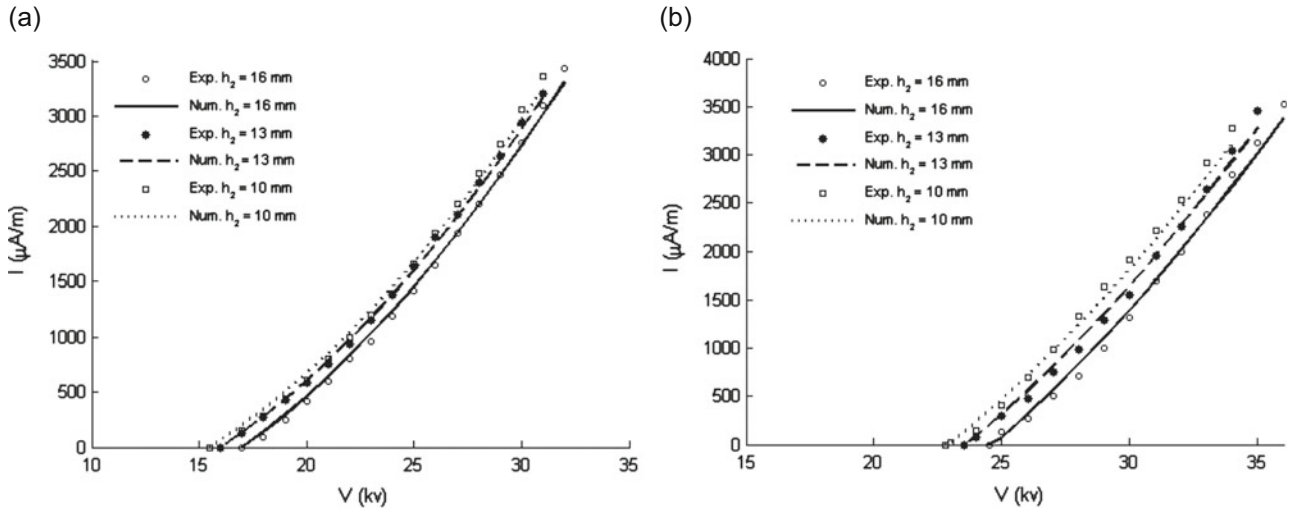

Fig. 6. Corona *V-I* characteristics of the Tri-electrode configuration for different wire diameters ($D = 25$ mm, $h_1 = 20$ mm). (a) $d_1 = d_2 = 0.3$ mm, (b) $d_1 = d_2 = 0.8$ mm.

6. Check for a self consistent electric field; if it is acceptable proceed to the next step. If not, modify the surface and space charges and go back to step 3 (inner loop).
7. Compute the average electric field at the ionizing wire. If it is acceptable compared with the onset value, then a self-consistent space charge field has been obtained and the solution is complete. If this field deviates from the onset value, modify the charge density distribution at the wire surface and go back to 3 (outer loop).

6 Characteristics of the Tri-electrode geometry

6.1 V-I Characteristic

The computed and measured current-voltage characteristic of the Tri-electrode geometry is shown in Figure 6. For a given wire diameter, the discharge current is influenced by the position of the auxiliary wire and increases as the distance h_2 decreases. At the same voltage, higher currents are obtained for smaller wire diameters. For the case $d_1 = d_2 = 0.3$ mm and at an applied voltage of 30 kV, the total discharge current increases by about 6% when h_2 changes from 16 mm to 13 mm and about 3% when h_2 changes from 13 mm to 10 mm. For the case $d_1 = d_2 = 0.8$ mm, the corresponding values are 18% and 10% respectively which demonstrate the effectiveness of the proposed system in controlling the discharge current. Less variation in the corona current is observed as the auxiliary wire moves up and away from the ionizing wire as the configuration becomes closer to perform as a dual electrode system. Experimental measurements are seen to be in good agreement with the numerical results.

6.2 Electric field

For different positions of the auxiliary wire, Figure 7 displays the variation of the computed electric field at the surface of the grounded plate at an applied voltage of 30 kV. As h_2 decreases, higher electric field values are obtained, with all other parameters being the same, and the distributions become relatively wider. For the case $d_1 = d_2 = 0.3$ mm, the maximum electric field rises by about 2% when h_2 varies from 16 mm to 10 mm and about 5% for the case $d_1 = d_2 = 0.8$ mm. The maximum charge Q_m to be acquired by a particle in a corona discharge is generally proportional to the maximum field strength which, in the present case, may be controlled by positioning the auxiliary wire farther away from the ionizing wire (h_2 decreases) at a given voltage.

6.3 Current density

The corresponding current density distributions are shown in Figure 8. For an applied voltage of 30 kV and $d_1 = d_2 = 0.3$ mm, the maximum current density grows by about 2.5% when h_2 moves from 16 mm to 10 mm and about 13.5% for the case $d_1 = d_2 = 0.8$ mm. Experimental measurements were found to be in good agreement with the results obtained using the developed numerical algorithm. It is observed that the spatial extension of theses quantities becomes smaller as the auxiliary wire moves closer (downward) to the ionizing wire. Apparently, the electric field lines (ions trajectories) are contracted and become more confined to a smaller region on the surface of the grounded electrode as h_2 increases. This means that the current density at the surface of the collecting electrode becomes larger or smaller, for a given corona current, depending on whether the auxiliary wire moves closer to the ionizing wire or farther away (upward) from it. Consequently, it is expected that the use of the proposed Tri-electrode system could provide better control over the acceleration of charge accumulation on the particles passing by the collecting electrode in a rather simple, fast and efficient manner.

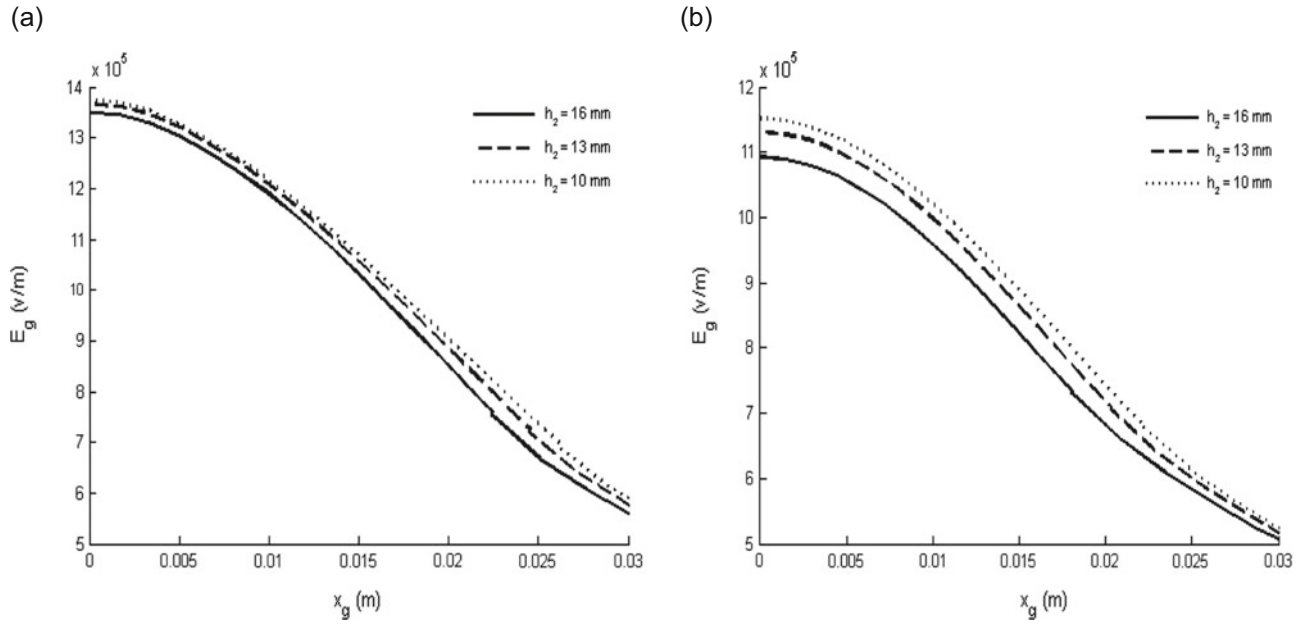

Fig. 7. Electric field distributions at the surface of the grounded plate for different locations of the auxiliary wire h_2 ($V = 30$ kV, $D = 25$ mm, $h_1 = 20$ mm). (a) $d_1 = d_2 = 0.3$ mm, (b) $d_1 = d_2 = 0.8$ mm.

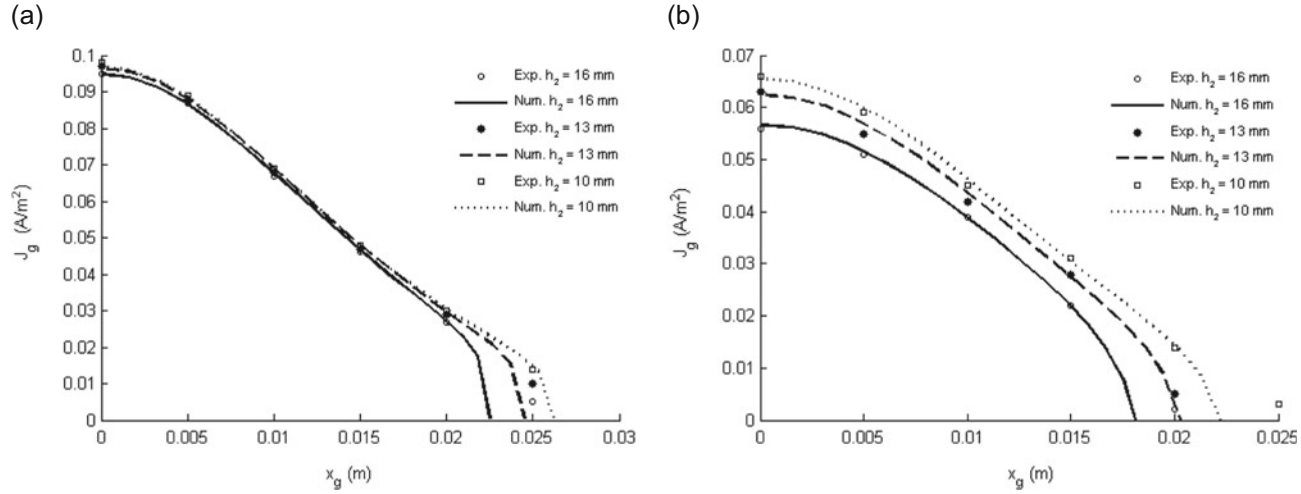

Fig. 8. Current density distributions at the surface of the grounded plate for different locations of the auxiliary wire h_2 ($V = 30$ kV, $D = 25$ mm, $h_1 = 20$ mm). (a) $d_1 = d_2 = 0.3$ mm, (b) $d_1 = d_2 = 0.8$ mm.

7 Discussion

In order to demonstrate the influence of Deutsch's assumption, maps for the space charge-free field (Laplace's equation) and the ion flow field (Poisson's equation) are presented in Figure 9. Field lines for the two cases are traced from the same starting points on the ionizing wire W_1 surface and the significant distorting effect of the space charge can be clearly seen. The large spreading of the ion flow field lines is more notable towards the edges of the charge-drift zone than that closer to the central axis. As the applied voltage increases from 26 to 30 kV, with the auxiliary wire midway between the ionizing wire and the cylinder, the spreading increases and the ion flow field lines cover a larger area of the collecting electrode, Figures 9a and 9b. The role played by the auxiliary wire is quite clear in Figures 9c and 9d. The field patterns become more confined to a smaller area on the collecting electrode when the auxiliary wire moves closer to the ionizing wire (h_2 changes from 10 mm to 16 mm). The distorting effect of the space charge on the field patterns of the present configuration is evident for the different cases considered as seen in Figure 9. These findings are consistent with the conclusions arrived at earlier [21,29,30], where it was reported that the use of Deutsch's assumption in the corona analysis is quite questionable and it may lead to significant inaccuracies in the paths along which ions flow from the wire to the collecting electrode.

For the same corona current, Figure 10 shows the current density distributions for different wire diameters.

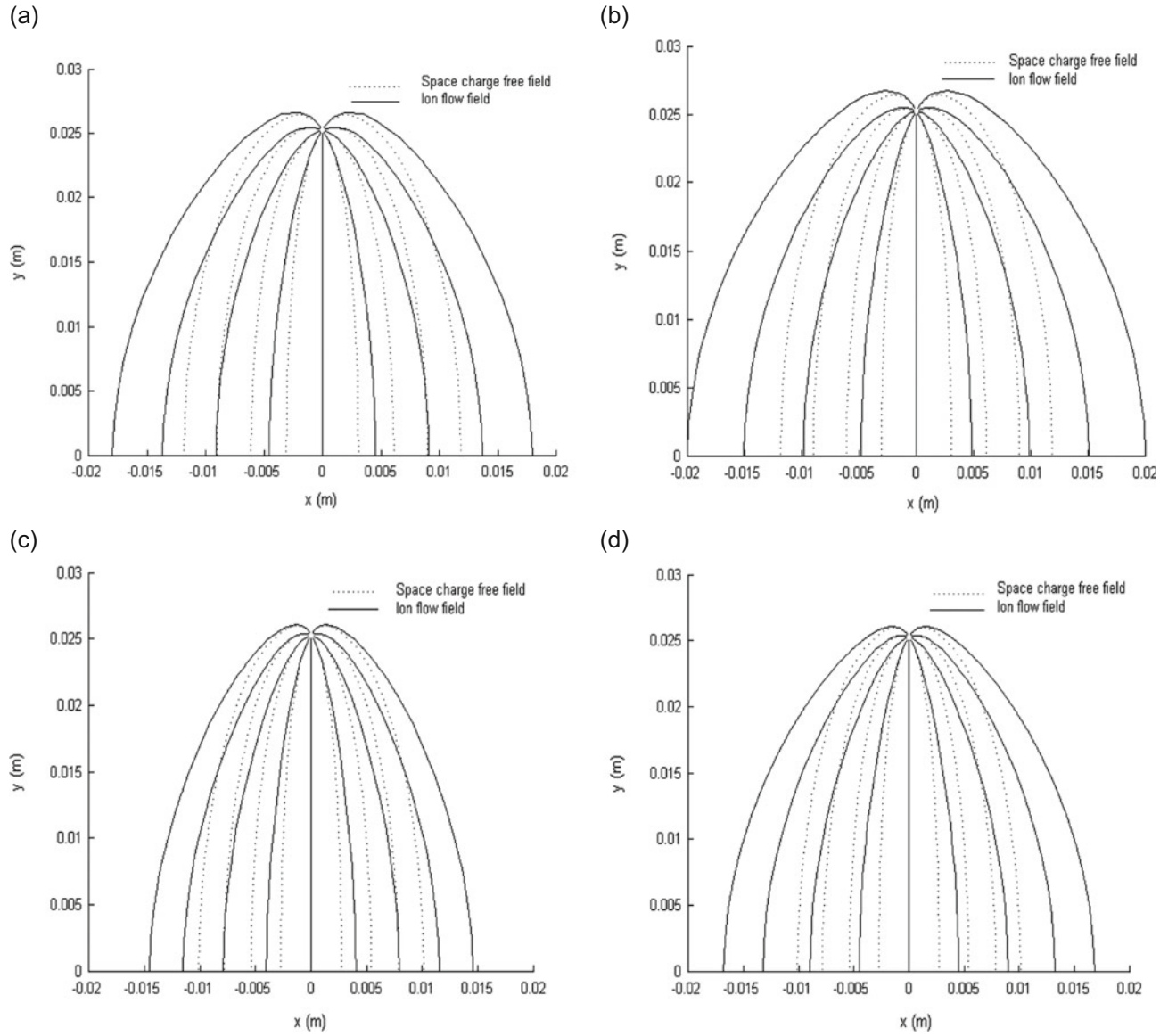

Fig. 9. Graphical comparison of the space charge-free field and the ion flow field patterns ($d_1 = d_2 = 0.5$ mm, $D = 25$ mm, $h_1 = 20$ mm). (a) $h_2 = 10$ mm, $V = 26$ kV; (b) $h_2 = 10$ mm, $V = 30$ kV; (c) $h_2 = 16$ mm, $V = 26$ kV; (d) $h_2 = 16$ mm, $V = 30$ kV.

These results clearly demonstrate the merits and versatility of the Tri-electrode system. Numerous profiles with different magnitudes as well as spatial extensions can be generated by simply positioning the auxiliary wire to meet the needs of various granular mixtures(fine particle, large flakes, etc.).

As the time constant of ionic charging is inversely proportional to the local density of the corona current [8,31]; then the generation of a current density distribution with a higher magnitude and narrower lateral extension, for a given corona current, may be favored to accelerate the accumulation of charge on the particles passing by the collecting electrode. This can be achieved with the present electrode system by using larger h_2 and larger wire diameters (e.g., $h_2 = 16$ mm and $d_1 = d_2 = 0.8$ mm in this case). On the other hand, the efficiency of the corona charging is usually estimated by studying the "pinning effect" that the electric image force has on charged insulating particles. Experimental studies [8,31] showed that, for the dual system, the "pinning effect" becomes stronger for large inter-electrode gap distances (ionizing wire to collecting plate). These results were related to the observation that the current density distributions become wider in this case even though the maximum current density values are lower. For the same corona current, moving the auxiliary wire up and away from the wire W_1 will extend the current density distribution further in order to meet these requirements even though its maximum value decreases. In brief, there will always be a "trade off" among the various parameters to control the separator's performance and to respond to the needs of separating different granular mixtures. For practical applications, these

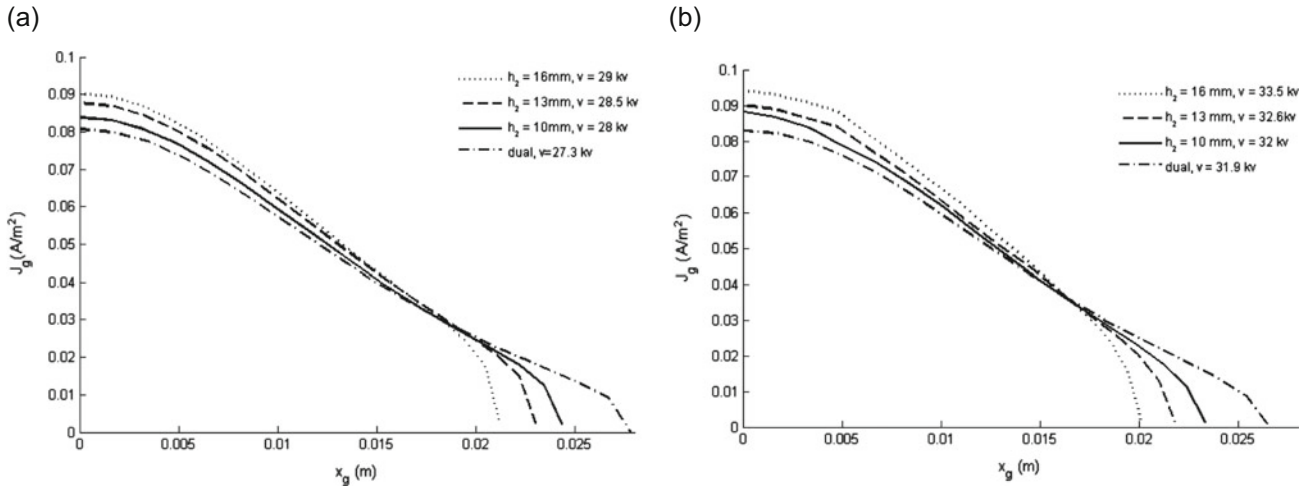

Fig. 10. Current density distributions at the surface of the grounded plate for same corona current ($D = 25$ mm, $h_1 = 20$ mm). (a) $d_1 = d_2 = 0.3$ mm, (b) $d_1 = d_2 = 0.8$ mm.

parameters could be easily adjusted and controlled according to the characteristics of each treated granular mixture for better separator's performance. The Tri-electrode system clearly provides the means for a more reliable and efficient operation of electrostatic separators. It is to be noted that, in the present case, the applied voltages are within 4–7% higher when compared with those of the dual electrode system; however they are still well within the voltage rating of high voltage supplies usually used in electrostatic separators (50–70 kV) [8,31].

8 Conclusions

The paper presented measurements and computations of the various corona characteristics of a new Tri-electrode system intended for electrostatic separation processes. The system aims to provide the means for a more efficient ion charging current; necessary for separation of different granular mixtures. Dependence of the voltage-current characteristics and spatial distributions of the electric field and current density on the system's geometrical parameters is examined and established both numerically and experimentally. A computational algorithm, not relying on Deutch's assumption, is developed to compute the associated ionized field quantities of the system. Mapping of the ion flow field patterns illustrates the impact of this assumption on the solution's accuracy. These field lines can be made to cover a wider or narrower area on the collecting electrode; not only by varying the applied voltage but also through adjustment of the auxiliary wire location. For the same corona current, various current density profiles, with different magnitudes as well as spatial extensions, can be generated by simply positioning the auxiliary wire to meet the needs of various granular mixtures (fine particle, large flakes, etc.). The numerical results were found to be, generally, in good agreement with the experimental data.

References

1. A.D. Moore (ed.), *Electrostatics and its Applications* (Wiley, New York, 1973)
2. J.S. Chang, A.J. Kelly, J.M. Crowley (eds.), *Handbook of Electrostatic Processes* (Dekker, New York, 1995)
3. J. Hughes, *Electrostatic Particle Charging* (Wiley, New York, 1997)
4. M. Kachi, M. Nemamcha, L. Herous, L. Dascalescu, J. Electrostat. **69**, 296 (2011)
5. B. Tabti, R. Mekideche, M. Plopeanu, L.M. Dumitran, L. Herous, L. Dascalescu, IEEE Trans. Ind. Appl. **46**, 634 (2010)
6. B. Tabti, L. Dascalescu, C.M. Plopeanu, A. Antoniu, R. Mekideche, J. Electrostat. **67**, 193 (2009)
7. L.M. Dumitran, O. Blejan, P.V. Notingher, A. Samuila, L. Dascalescu, IEEE Trans. Ind. Appl. **44**, 1385 (2008)
8. A. Samuila, M. Blajan, R. Beleca, M. Huzau, R. Morar, L. Dascalescu, A. Iuga, J. Electrostat. **63**, 955 (2005)
9. D. Rafiroiu, I. Suarasan, R. Morar, P. Atten, L. Dascalescu, IEEE Trans. Ind. Appl. **37**, 766 (2001)
10. M. Abouelsaad, M. Abouelatta, A. Salama, IET Sci. Meas. Technol. **7**, 16 (2012)
11. D. Rafiroiu, R. Morar, P. Atten, L. Dascalescu, IEEE Trans. Ind. Appl. **36**, 1260 (2000)
12. L.M. Dumitram, P. Atten, P.V. Notingher, L. Dascalescu, J. Electrostat. **64**, 176 (2005)
13. L. Dascalescu, A. Iuga, R. Morar, V. Neamtu, I. Suarran, A. Samuila, D. Rafiroiu, J. Electrostat. **29**, 211 (1993)
14. L. Dascalescu, A. Samuila, D. Rafiroiu, A. Iuga, R. Morar, IEEE Trans. Ind. Appl. **35**, 543 (1999)
15. A. Iuga, A. Samuila, M. Blajan, R. Beleca, R. Morar, L. Dascalescu, Characterization of wire corona electrodes at various discharge gaps in electrostatic separation processes, in *39th IAS Annual Meeting. Industry Applications Conference, Seattle, USA, 2004*
16. L.M. Dumitran, L. Dascalescu, P.V. Notingher, P. Atten, J. Electrostat. **65**, 758 (2007)
17. M.C. Plopeanu, L. Dascalescu, B. Yahiaoui, A. Antoniu, M. Hulea, P. Notingher, IEEE Trans. Ind. Appl. **48**, 851 (2012)

18. M.C. Plopeanu, L. Dascalescu, B. Neagoe, A. Bendaoud, P. Notingher, J. Electrostat. **71**, 517 (2013)
19. M. Kachi, L. Dascalescu, J. Electrostat. **72**, 6 (2014)
20. M. Abouelsaad, IET Sci. Meas. Technol. **8**, 1 (2014)
21. R.S. Sigmond, J. Electrostat. **18**, 249 (1986)
22. F. Peek, *Ionization Phenomena in High Voltage Engineering* (McGraw-Hill, New York, 1929)
23. P. Sattari, C.F. Gallo, G.S.P. Castle, K. Adamiak, J. Phys. D: Appl. Phys. **44**, 5502 (2011)
24. K. Yanallah, F. Pontiga, A. Castellanos, J. Phys. D: Appl. Phys. **44**, 5201 (2011)
25. V. Jaiswal, M.J. Thomas, J. Phys. D: Appl. Phys. **36**, 3089 (2003)
26. K. Yanallah, F. Pontiga, Plasma Sources Sci. Technol. **21**, 5007 (2012)
27. M. Abdel-Salam, A. Hashem, A. Turky, A. Abdel Aziz, J. Phys. D: Appl. Phys. **40**, 1684 (2007)
28. A.A. Elmoursi, C.E. Speck, IEEE Trans. Ind. Appl. **26**, 384 (1990)
29. J.E. Jones, M. Davies, J. Phys. D: Appl. Phys. **25**, 1749 (1992)
30. A. Bouziane, K. Hidaka, J.E. Jones, A.R. Rowlands, M.C. Taplamacioglu, R.T. Waters, IEE Proc.-Sci. Meas. Technol. **141**, 205 (1994)
31. A. Bendaoud, A. Tilmatine, K. Medles, M. Rahli, M. Huzau, L. Dascalescu, IEEE Trans. Ind. Appl. **44**, 692 (2008)